Nonreciprocal enhancement of macroscopic entanglement with noise tolerance

Z.-H. Huang,[1] Y.-F. Jiao,[2,3] L.-L. Yan,[1,4] D.-Y. Wang,[1,*] S.-L. Su,[1,4] and Hui Jing[2,5,†]

[1]*School of Physics, Zhengzhou University, Zhengzhou, Henan 450001, People's Republic of China*

[2]*Academy for Quantum Science and Technology, Zhengzhou University of Light Industry, Zhengzhou 450002, People's Republic of China*

[3]*School of Electronics and Information, Zhengzhou University of Light Industry, Zhengzhou 450001, People's Republic of China*

[4]*Institute of Quantum Materials and Physics, Henan Academy of Sciences, Zhengzhou 450046, People's Republic of China*

[5]*Key Laboratory of Low-Dimensional Quantum Structures and Quantum Control of Ministry of Education, Department of Physics and Synergetic Innovation Center for Quantum Effects and Applications, Hunan Normal University, Changsha, Hunan 410081, People's Republic of China*

(Received 25 January 2024; accepted 18 June 2024; published 8 July 2024)

The entanglement of different macroscopic objects can provide crucial resources for various quantum applications and quantum-enabled devices. The generation, manipulation, and enhancement of entanglement are pivotal areas of research. In this study, we introduce an approach for producing enhanced nonreciprocal entanglement in a hybrid spinning optomechanical system. By exploiting the Sagnac effect to break the time-reversal symmetry of the system, we successfully generate and amplify the nonreciprocal bipartite entanglement between the atomic ensemble and mechanical oscillator, exhibiting an approximately twofold enhancement under competitive equilibrium conditions. Furthermore, we investigate and quantify the nonreciprocal tripartite entanglement encompassing the atomic ensemble, optical cavity, and mechanical oscillator by employing the residual contangle measurement. We find that the nonreciprocal bipartite (tripartite) entanglement is not only enlarged almost two (five) times, but also noise resistant. The proposed scheme of enhanced bipartite and tripartite entanglement has the potential to advance a wide range of quantum technologies, spanning from quantum information processing to quantum sensing applications.

DOI: 10.1103/PhysRevA.110.012423

I. INTRODUCTION

Entanglement, a characteristic phenomenon of the intricate quantum domain [1–3], serves as a fundamental resource for advancing quantum technologies such as quantum communications [4], quantum information processing [5–7], and quantum sensing [8]. Initially, researchers concentrated on preparing, manipulating, and quantifying quantum entanglement solely within microscopic systems encompassing entities such as photons, atoms, and ions [9]. However, with notable progress in microfabrication, the exploration of entanglement among macroscopic entities has garnered significant interest and is now evolving [10–12]. Recent experimental breakthroughs in macroscopic entanglement have been witnessed across a spectrum of systems, including the single-particle interference of macromolecules [13], the collective spins of atomic ensembles [14], the superconducting microcircuit [15,16], and beyond. In recent times, cavity optomechanical (COM) systems have emerged as a primary platform for investigating macroscopic quantum phenomena [17–19]. This rapidly advancing frontier in research delves into fundamental macroscopic physical phenomena driven by optomechanical interactions [20–26]. Extensive exploration of fundamental quantum theory within this domain includes studies of macroscopic quantum coherence [27], quantum sensing [26,28], and quantum-classical boundary [19]. Due to the advantages of universality and scalability, the COM platform offers broad applications in modern quantum sciences and technologies, including quantum precision measurements [29] and gravitational wave detection [30]. With the rapid advancement of this field in recent years, diverse research directions within COM systems have emerged. Among these, the exploration of quantum entanglement between optical cavities and mechanical resonators stands out as particularly intriguing [3]. Recently, a variety of schemes has been proposed, aiming to achieve macroscopic entanglement [21–24,31–35] and hybrid multiparticle entanglement through the integration of atoms, ions, or additional mechanical oscillators [36–40].

In parallel with the rapid development of the COM system, nonreciprocal physics has also witnessed significant breakthroughs in recent years. Various methods for fabricating nonreciprocal optical devices have been proposed and demonstrated both theoretically and experimentally [41–49]. These nonreciprocal optical devices have crucial applications in numerous areas, including optical chaos [18], unidirectional laser [50,51], optomechanical high-order sidebands [18], one-way photon blockade [52–54], single-photon isolator [55–57], and nonreciprocal entanglement [58,59]. The intersection of nonreciprocal physics and quantum entanglement has led to the emergence of numerous promising schemes across various systems. Recently, several approaches to achieve nonreciprocal entanglement between different modes have been proposed [58–63]. However, here we explore the concept of nonreciprocal enhancement of macroscopic entanglement.

*Contact author: dywang@zzu.edu.cn

†Contact author: jinghui73@gmail.com

In this paper, we propose a scheme to achieve enhanced nonreciprocal bipartite and tripartite macroscopic entanglement in a spinning COM system [59,64], exploiting the Sagnac effect to break time-reversal symmetry. Our work demonstrates that both bipartite and tripartite entanglement are significantly enhanced under nonreciprocal conditions. We delve into the intrinsic mechanisms underlying this enhancement, attributing it to greater entanglement transfer when the system's internal coupling reaches competitive equilibrium. Additionally, we investigate the robustness of nonreciprocal macroscopic entanglement against environmental noise, finding that the achieved nonreciprocal bipartite and tripartite entanglement exhibit higher noise tolerance. Our proposal offers the following features: (i) achievement of nonreciprocal bipartite and tripartite macroscopic entanglement, (ii) significant enhancement of macroscopic entanglement compared to traditional schemes, and (iii) superior noise tolerance of nonreciprocal bipartite and tripartite entanglement compared to stationary systems. This proposal provides valuable resources for engineering various quantum effects, such as establishing viable phononic quantum networks, synchronizing mechanical motions, realizing dual-comb spectroscopy, and advancing chiral quantum information processing [19,65–67].

This paper is structured as follows. In Sec. II, we introduce the theoretical model and the derivation of the linearized dynamics and quantification of the quantum entanglement. In Sec. III, by applying the logarithmic negativity and residual contangle, we demonstrate the enhanced bipartite and tripartite entanglement in the nonreciprocal effect. In Sec. IV, we briefly discuss the experimental feasibility based on two possible schemes. A summary is given in Sec. V.

II. THEORETICAL MODEL AND ENTANGLEMENT QUANTIFICATION

Our theoretical model is a hybrid optomechanical system, where an atomic ensemble is directly or indirectly coupled with a whispering gallery microresonator (WGM). The resonator is mounted on a turbine [68] and evanescently coupled to a tapered fiber. Here, the atomic ensemble consists of N_a two-level atoms with natural frequency ω_a. By inputting the laser from opposite directions, we can drive two different cavity propagating modes, i.e., clockwise (CW) mode and counterclockwise (CCW) mode. In addition, the spinning resonator can be flexibly stretched, providing a mechanical breathing mode with frequency ω_m.

For the spinning resonator, the system's time-reversal symmetry has been broken due to the Sagnac-Fizeau shift [69],

$$\Delta_F = \frac{nR\Omega\omega_c}{c}\left(1-\frac{1}{n^2}-\frac{\lambda}{n}\frac{dn}{d\lambda}\right), \tag{1}$$

where ω_c is the stationary resonance frequency. The wavelength and the speed of light in vacuum are λ and c, respectively. The radius and the angular velocity of the resonator are R and Ω, respectively. The refractive index of the material is n. The dispersion term $dn/d\lambda$, which is small in the typical materials (up to 0.01 m^{-1}), indicates the relativistic origin of the Sagnac effect [68,69]. Meanwhile, the effective cavity frequency of the CW (CCW) driving mode is given by $\omega_{cw} = \omega_c + \Delta_F$ ($\omega_{ccw} = \omega_c - \Delta_F$).

When the CCW mode is driven by a laser field, the system can be described by the Hamiltonian

$$\begin{aligned} H &= H_0 + H_I, \\ H_0 &= \sum_{j=ccw,cw}\hbar\omega_j a_j^\dagger a_j + \frac{\hbar\omega_m}{2}(p^2+q^2) + \frac{\hbar\omega_a}{2}S_z, \\ H_I &= -\hbar G_0(a_{cw}^\dagger a_{cw} + a_{ccw}^\dagger a_{ccw})q + (\hbar g a_{cw} S_+ \\ &\quad + \hbar g a_{ccw} S_+ + i\hbar\epsilon e^{-i\omega_0 t}a_{ccw}^\dagger + \mathrm{H.c.}). \end{aligned} \tag{2}$$

On the other side, when the laser is used to drive the CW mode, the driving term $i\hbar\epsilon e^{-i\omega_0 t}a_{ccw}^\dagger$ needs to be substituted to $i\hbar\epsilon e^{-i\omega_0 t}a_{cw}^\dagger$. Here, $S_{\pm,z} = \sum_{i=1}^{N_a}\sigma_{\pm,z}^i$ are the collective spin operators of the atomic ensemble, where σ_+, σ_-, and σ_z are the spin-1/2 algebra Pauli matrices. The annihilation and creation operators of cavity mode j are a_j and $a_j^\dagger$. The dimensionless mechanical displacement and momentum operators are q and p. The single-photon optomechanical coupling constant is given by $G_0 = (\omega_c/R)\sqrt{\hbar/m\omega_m}$, where m is the mass of the resonator [17]. Similarly, the atom-cavity coupling constant is given by $g = \mu\sqrt{\omega_c/2\hbar\epsilon_0 V}$, where V is the cavity mode volume and μ is the dipole moment of the atomic transition. The field amplitude of the input laser is $|\epsilon| = \sqrt{2\kappa P/\hbar\omega_0}$ with frequency $\omega_0 = 2\pi c/\lambda = 1.216\times10^{15}$ Hz, where κ and P are the optical decay rate and input laser power. In a rotating frame with respect to $H_i = \hbar\omega_0(a_{cw}^\dagger a_{cw} + a_{ccw}^\dagger a_{ccw} + S_+S_-)$, the Hamiltonian changes [17],

$$\begin{aligned} H &= \sum_{j=cw,ccw}\hbar\Delta_j a_j^\dagger a_j + \hbar\Delta_a S_+S_- + \frac{\hbar\omega_m}{2}(p^2+q^2) \\ &\quad - \hbar G_0(a_{cw}^\dagger a_{cw} + a_{ccw}^\dagger a_{ccw})q + (\hbar g a_{cw}S_+ \\ &\quad + \hbar g a_{ccw}S_+ + i\hbar\epsilon a_{ccw}^\dagger + \mathrm{H.c.}), \end{aligned} \tag{3}$$

where $\Delta_j = \omega_j - \omega_0$ and $\Delta_a = \omega_a - \omega_0$ are the effective detuning. The spin operators $S_{\pm,z}$ of the atomic ensemble can be transformed to a collective bosonic operator $c^\dagger(c)$ in the Holstein-Primakoff representation [39,70,71],

$$\begin{aligned} S_- &= c\sqrt{N_a - c^\dagger c} \approx \sqrt{N_a}c, \\ S_+ &= c^\dagger\sqrt{N_a - c^\dagger c} \approx \sqrt{N_a}c^\dagger, \\ S_z &= c^\dagger c - \frac{N_a}{2}, \end{aligned} \tag{4}$$

where the operators c and $c^\dagger$ obey the standard boson commutator $[c,\ c^\dagger] = 1$. This is satisfied under the low temperature (low excitation limit), i.e., $\langle c^\dagger c\rangle/N_a \ll 1$.

Considering the photon losses in the cavity, the spontaneous emission of atoms, and the Brownian noise acting on the mirror, we can get the quantum Langevin equation as follows:

$$\begin{aligned} \dot{q} &= \omega_m p, \\ \dot{p} &= -\omega_m q + G_0(a_{cw}^\dagger a_{cw} + a_{ccw}^\dagger a_{ccw}) - \gamma_m p + \xi, \\ \dot{a}_{cw} &= -(i\Delta_{cw} + \kappa)a_{cw} + iG_0 q a_{cw} - iG_a c + \sqrt{2\kappa}a_{cw}^{in}, \\ \dot{a}_{ccw} &= -(i\Delta_{ccw} + \kappa)a_{ccw} + iG_0 q a_{ccw} - iG_a c + \sqrt{2\kappa}a_{ccw}^{in} + \epsilon, \\ \dot{c} &= -(i\Delta_a + \gamma_a)c - iG_a(a_{cw} + a_{ccw}) + \sqrt{2\gamma_a}F_c, \end{aligned} \tag{5}$$

where γ_m and γ_a are the mechanical damping rate and the line width of the atomic excited state. The coupling constant between the CW (CCW) optical mode and atomic mode is G_{cw-a} (G_{ccw-a}). For simplicity, the effective atomic coupling constant is set as $G_{cw-a} = G_{ccw-a} = G_a = g\sqrt{N_a}$ in our proposal. The zero-mean input noise operators for the optical, atomic, and mechanical modes are a_j^{in}, F_c, and ξ, respectively. Under the condition of $\omega_m/\gamma_m \gg 1$, these noise operators can be described by the following correlation functions [72]:

$$\begin{aligned}\left\langle a_j^{in}(t)a_j^{in,\dagger}(t')\right\rangle &= \delta(t-t'),\\ \langle F_c(t)F_c^{\dagger}(t')\rangle &= \delta(t-t'),\\ \langle \xi(t)\xi(t')\rangle &\simeq \gamma_m(2n_m+1)\delta(t-t'),\end{aligned} \tag{6}$$

where n_m is the thermal phonon number and characterized by the equation $n_m = [\exp(\hbar\omega_m/k_BT - 1)]^{-1}$, with the k_B the Boltzmann constant and T the temperature of the mechanical oscillator reservoir.

Under the strong optical driving, we can linearize these operators by separating them into two parts, i.e., a steady-state value plus a small fluctuation, i.e., $q = q_s + \delta q$, $p = p_s + \delta p$, $a_j = \alpha_j + \delta a_j$, $c = c_s + \delta c$. The quadratures of fluctuation and noise operators are defined by

$$\begin{aligned}\delta X_j &= \frac{1}{\sqrt{2}}(\delta a_j^{\dagger} + \delta a_j), \quad \delta Y_j = \frac{i}{\sqrt{2}}(\delta a_j^{\dagger} - \delta a_j),\\ \delta x &= \frac{1}{\sqrt{2}}(\delta c^{\dagger} + \delta c), \quad \delta y = \frac{i}{\sqrt{2}}(\delta c^{\dagger} - \delta c),\\ X_j^{in} &= \frac{1}{\sqrt{2}}\left(a_j^{in,\dagger} + a_j^{in}\right), \quad Y_j^{in} = \frac{i}{\sqrt{2}}\left(a_j^{in,\dagger} - a_j^{in}\right),\\ x_{in} &= \frac{1}{\sqrt{2}}\left(F_c^{in,\dagger} + F_c^{in}\right), \quad y_{in} = \frac{i}{\sqrt{2}}\left(F_c^{in,\dagger} - F_c^{in}\right).\end{aligned} \tag{7}$$

We define the vectors of the quadratures of fluctuation operators and operators of input noises, $u^T(t) = (\delta X_{ccw}, \delta Y_{ccw}, \delta X_{cw}, \delta Y_{cw}, \delta x, \delta y, \delta q, \delta p)$ and $v^T(t) = (\sqrt{2\kappa}X_{ccw}^{in}, \sqrt{2\kappa}Y_{ccw}^{in}, \sqrt{2\kappa}X_{cw}^{in}, \sqrt{2\kappa}Y_{cw}^{in}, \sqrt{2\gamma_a}x_{in}, \sqrt{2\gamma_a}y_{in}, 0, \xi)$. Equation (5) can be written in compact form as $\dot{u}(t) = Au(t) + v(t)$, where

$$A = \begin{pmatrix} -\kappa & \tilde{\Delta}_{ccw} & 0 & 0 & 0 & G_a & -G_{ccw}^{y} & 0\\ -\tilde{\Delta}_{ccw} & -\kappa & 0 & 0 & -G_a & 0 & G_{ccw}^{x} & 0\\ 0 & 0 & -\kappa & \tilde{\Delta}_{cw} & 0 & G_a & -G_{cw}^{y} & 0\\ 0 & 0 & -\tilde{\Delta}_{cw} & -\kappa & -G_a & 0 & G_{cw}^{x} & 0\\ 0 & G_a & 0 & G_a & -\gamma_a & \Delta_a & 0 & 0\\ -G_a & 0 & -G_a & 0 & -\Delta_a & -\gamma_a & 0 & 0\\ 0 & 0 & 0 & 0 & 0 & 0 & 0 & \omega_m\\ G_{ccw}^{x} & G_{ccw}^{y} & G_{cw}^{x} & G_{cw}^{y} & 0 & 0 & -\omega_m & -\gamma_m \end{pmatrix}. \tag{8}$$

Here, we have redefined the effective optical detuning $\tilde{\Delta}_j = \Delta_j - G_0 q_s$. The real and imaginary parts of the linearized optomechanical coupling strength are G_j^x and G_j^y, i.e., $G_{j-m} = G_j^x + iG_j^y = \sqrt{2}G_0\alpha_j$. The linearized optomechanical coupling strength for the CW optical mode and CCW optical mode are G_{cw-m} and G_{ccw-m}, respectively. The solution of the above compact form equation can be given directly,

$$u(t) = M(t)u(0) + \int_0^t dsM(s)v(t-s), \tag{9}$$

where $M(t) = \exp(At)$. According to the Routh-Hurwitz criterion [73], the system eventually reaches stability only when all eigenvalues of A have the negative real parts. In our proposed parameter scheme, the criterion can be satisfied. Meanwhile, the steady-state value of the system operators is given by

$$\begin{aligned}p_s &= 0,\\ q_s &= \frac{G_0(|\alpha_{cw}|^2 + |\alpha_{ccw}|^2)}{\omega_m},\\ \alpha_{cw} &= \frac{-iG_a c_s}{i\tilde{\Delta}_{cw} + \kappa},\\ \alpha_{ccw} &= \frac{-iG_a c_s + \epsilon}{i\tilde{\Delta}_{ccw} + \kappa},\\ c_s &= \frac{-iG_a(\alpha_{ccw} + \alpha_{cw})}{i\Delta_a + \gamma_a}.\end{aligned} \tag{10}$$

The steady state is independent of the initial condition.

Due to the quantum noise terms having a Gaussian nature and the system dynamics being linearized, we can use an 8×8 correlation matrix to characterize the steady state of the system, which is a zero-mean four-partite Gaussian state. The correlation matrix is given by

$$V_{kl} = \frac{\langle u_k(\infty)u_l(\infty) + u_l(\infty) + u_k(\infty)\rangle}{2}. \tag{11}$$

Because the system can be stable eventually after the long evolution, we get $M(\infty) = 0$ and $u(\infty) = \int_0^{\infty} dsM(s)n(t-s)$. By substituting this result into Eq. (11), the Lyapunov equation of the system is given as follows [3]:

$$AV + VA^T = -D, \tag{12}$$

where $D = \mathrm{diag}[\kappa, \kappa, \kappa, \kappa, \gamma_a, \gamma_a, 0, \gamma_m(2n_m+1)]$ is the diffusion matrix. By solving Eq. (12), we can get the correlation matrix V which includes internal information of the correlation. The correlation matrix V can be described in this

way [74],

$$V = \begin{pmatrix} K_{ccw} & L_{ccw-cw} & L_{ccw-a} & L_{ccw-m} \\ L^T_{ccw-cw} & K_{cw} & L_{cw-a} & L_{cw-m} \\ L^T_{ccw-a} & L^T_{cw-a} & K_a & L_{a-m} \\ L^T_{ccw-m} & L^T_{cw-m} & L^T_{a-m} & K_m \end{pmatrix}, \tag{13}$$

where each matrix element represents a 2×2 matrix, e.g., K_{ccw} and K_{cw} are used to describe the local characters of two cavity modes with different driving directions. K_a and K_m describe the atomic mode and mechanical mode. L_{i-j}, respectively, describes the correlation of two modes ($i, j = ccw, cw, a, m$). By adopting the logarithmic negativity E_{i-j}, we quantify the bipartite entanglement between any two components. For example, the bipartite entanglement between any two modes can be defined as [75]

$$E_{i-j} = \max[0, -\ln 2\mu^-], \tag{14}$$

where $\mu^- = \min[\mathrm{eig}(i\Omega_2 \tilde{V}_4)]$, $\Omega_2 = \bigoplus_{j=1}^{2} i\sigma_y$, and $\tilde{V}_4 = P_{1|2} V_4 P_{1|2}$ [36,76,77]. Here, $P_{1|2} = \mathrm{diag}(1, -1, 1, 1)$ and V_4 is the correlation matrix of a two-mode subsystem. When we study the bipartite entanglement between the mechanic mode and the atomic mode, the correlation matrix V_4 is

$$V_{a-m} = \begin{pmatrix} K_a & L_{a-m} \\ L^T_{a-m} & K_m \end{pmatrix}. \tag{15}$$

For a Gaussian state of the two-mode system, entanglement can be generated if and only if $\mu^- < 1/2$, which is equivalent to Simon's entanglement criterion [76].

Moreover, by applying a contangle quantity, we can quantify tripartite entanglement. The definition of contangle is given by [78,79]

$$R^{i|jk}_{\mathcal{T}} = C_{i|jk} - C_{i|j} - C_{i|k}, \tag{16}$$

where $C_{u|v}$ is defined as the squared logarithmic negativity and is used to quantify the entanglement of the subsystem which consists of u and v. Here, v can contain one mode or two modes. To calculate the one-mode–vs–two mode contangle $C_{i|jk}$, Eq. (14) can be applied, but $\Omega_2 = \bigoplus_{j=1}^{2} i\sigma_y$ needs to be substituted to $\Omega_3 = \bigoplus_{j=1}^{3} i\sigma_y$ as well as $\tilde{V}_4 = P_{1|2} V_4 P_{1|2}$ is substituted to $\tilde{V} = P_{i|jk} V_6 P_{i|jk}$, where

$$\begin{aligned} P_{1|23} &= \mathrm{diag}(1, -1, 1, 1, 1, 1), \\ P_{2|13} &= \mathrm{diag}(1, 1, 1, -1, 1, 1), \\ P_{3|12} &= \mathrm{diag}(1, 1, 1, 1, 1, -1). \end{aligned} \tag{17}$$

The monogamy of quantum entanglement is satisfied, $R^{i|jk}_{\mathcal{T}} \geqslant 0$, i.e.,

$$C_{i|jk} \geqslant C_{i|j} + C_{i|k}, \tag{18}$$

which is similar to the Coffman-Kundu-Wootters monogamy inequality of a three-qubit system [80]. The tripartite entanglement can be quantified by the minimum residual contangle, which can be defined as follows [78,79]:

$$R_{\mathcal{T}} = \min\left[R^{a|mb}_{\mathcal{T}}, R^{m|ab}_{\mathcal{T}}, R^{b|am}_{\mathcal{T}}\right]. \tag{19}$$

The nonzero $R_{\mathcal{T}}$ denotes that the genuine tripartite entanglement is generated in the system.

III. NONRECIPROCAL ENHANCEMENT OF ENTANGLEMENT

In this section, the logarithmic negativity and the minimum residual contangle are, respectively, applied to quantify the bipartite and tripartite entanglement of different modes (cavity mode, mechanical mode, and atomic mode). And we investigate the variation of entanglement with the change of parameter conditions. The most remarkable part of our system is the enhanced nonreciprocal entanglement.

A. Bipartite entanglement

We first compare and discuss the variation of the bipartite entanglement, and atom-mechanical entanglement E_{a-m}, with respect to the stationary resonator and spinning resonator driven by the input laser in opposite directions, respectively. As shown in Fig. 1(c), the logarithmic negativity of atom-mechanical subsystem E_{a-m} as a function of the cavity field detuning is plotted with choosing experimental feasible parameters: $n = 1.48$, $m = 10$ ng, $R = 1.1$ mm, $\lambda = 1550$ nm, $Q = 3.2 \times 10^7$, $\omega_m = 63$ MHz, $\gamma_m = 5.2$ kHz, $T = 5$ mK, $\Omega = 30$ kHz, $\kappa = \gamma_a = 38$ MHz, $P = 40$ mW, $G_a/\omega_m = 0.6$, $\Delta_a/\omega_m = -1.1$.

When the resonator is stationary, the time-reversal symmetry of the system is unbroken, and the entanglement between the atomic ensemble and mechanical oscillator is constant for the opposite direction driving, i.e., an identical effect can be achieved whether or not the CW or CCW cavity mode is driven. Meanwhile, the maximal value of atom-mechanical entanglement occurs around $\Delta_c/\omega_m \simeq 1$. The optimal cavity detuning for atom-mechanical entanglement in the optomechanical system is at the red-sideband resonance, which has been extensively investigated and discussed [39,78]. The underlying physics can be attributed to the redistribution of bipartite entanglement. On the other hand, when the resonator rotates in a counterclockwise direction and is, respectively, driven from both sides, the effective frequency of the optic cavity is shifted due to the Sagnac effect ($\omega_c \pm \Delta_F$). Meanwhile, the atom-mechanical entanglement is different for the spinning resonator with driving the CW and CCW modes, which shows that we achieve the nonreciprocal entanglement between two macroscopic objects. As shown in Fig. 1(c), the peak of entanglement is shifted into opposite directions [59]. Except for the change of the optimal cavity detuning condition due to the Sagnac effect, we also find that the maximal value of atom-mechanical entanglement is significantly enhanced, e.g., surpassing near 1.72 times with driving CW mode and near 1.8 times with driving CCW mode compared to the atom-mechanical entanglement of the stationary resonator.

To explain the enhancement effect of nonreciprocal entanglement in our proposal, we traverse all the bipartite entanglement of the subsystems and give an intrinsic physical reason. Those results are shown in Figs. 2(a)–2(c), where we plot the logarithmic negativity of different two-mode subsystems versus the atom detuning Δ_a. In Fig. 2(a), the cavity detuning is set to $\Delta_c/\omega_m \simeq 1$, i.e., the optimal cavity detuning condition for the stationary resonator coming from Fig. 1. It is noticed that the entanglement is redistributed from the cavity-mechanical subsystem to the atom-cavity and the

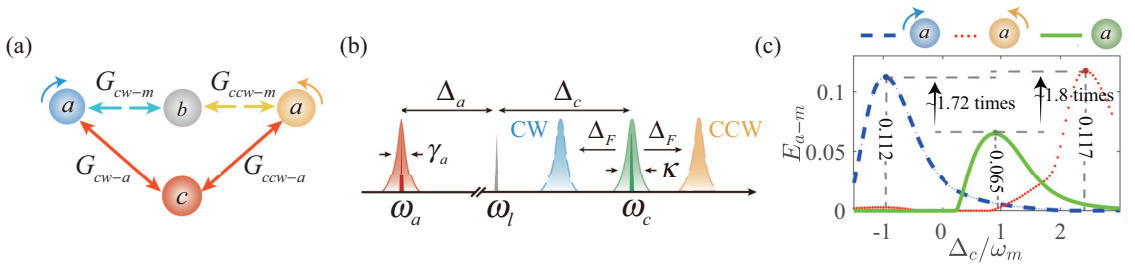

FIG. 1. (a) The coupling strength between different modes. Due to the presence of an atomic ensemble, the entanglement between the driving cavity mode and mechanical mode is redistributed to the entanglement between other modes so that the four modes can be coupled together. (b) Frequency spectrum of the spinning COM system. The effective frequency of the optical cavity is shifted into opposite directions ($\omega_c + \Delta_F$ and $\omega_c - \Delta_F$) due to the Sagnac effect. (c) Nonreciprocal enhancement of entanglement between atomic ensemble and mechanical oscillator. The parameters are chosen as $\Omega = 30$ kHz, $\Delta_a/\omega_m = -1.1$, $G_a/\omega_m = 0.6$, and $P = 40$ mW.

atom-mechanical subsystems near $\Delta_a/\omega_m \simeq -1$. In addition, it is found that due to the indirect interaction induced by atoms, the entanglement can also be redistributed to that undriven cavity-atom mode and undriven cavity-mechanical mode, as shown in the green lines in Fig. 2(a). As a result, the four modes in the system are entangled between two pairs, and the schematic diagram is shown in Fig. 1(a). In Figs. 2(b) and 2(c), the resonator remains spinning and the system is, respectively, driven from the opposite directions. Meanwhile, the optimal cavity detuning conditions for different driving situations are different and satisfied, respectively, i.e., $\Delta_c/\omega_m \simeq -1$ for CW mode driven and $\Delta_c/\omega_m \simeq 2.5$ for CCW mode driven. Compared with the stationary resonator in Fig. 2(a), we find that the entanglement redistribution from the driven cavity-mechanical mode to the atomic-mechanical mode becomes more significant, and other unimportant entanglement is restrained. Therefore, the atom-mechanical entanglement is enhanced at the optimal detuning.

In addition, we further investigate the underlying reason for the enhancement of entanglement redistribution in our proposal. In Figs. 2(d)–2(f), we show the effective strengths of driven optomechanical coupling $G_{cw(ccw)-m}$ and cavity-atom coupling $G_{cw(ccw)-a}$ versus the atom detuning Δ_a, where the cavity field detuning is set to the optimal conditions in different driving situations. Here, the cavity-atom coupling strength is assumed to be constant and does not vary with the atom detuning. However, the effective optomechanical coupling strength $G_{cw(ccw)-m} = \sqrt{2}G_0\alpha_{cw(ccw)}$ varies with the change of atom detuning, which is evident from Eq. (11). In Figs. 2(e) and 2(f), the resonator remains spinning and the system is, respectively, driven from the opposite directions. We can see that the effective optomechanical coupling strength is close to the cavity-atom coupling at $\Delta_a/\omega_m \simeq -1$, while the values of these two coupling strengths are separated for the stationary resonator at $\Delta_a/\omega_m \simeq -1$, as shown in Fig. 2(d). When entanglement redistribution emerges, the approximately equal coupling strengths can enhance the entanglement transfer process, contributing to the more significant entanglement redistribution in the nonreciprocal effect. That is to say, the entanglement transfer is most remarkable when the coupling is in equilibrium.

In Fig. 3, we, respectively, plot E_{a-m} versus the decay of cavity κ and the spontaneous radiation of atom γ_a in different driving situations, where the optimal cavity and atomic detuning conditions for different driving situations have been satisfied. We can see that the nonreciprocal atom-mechanical

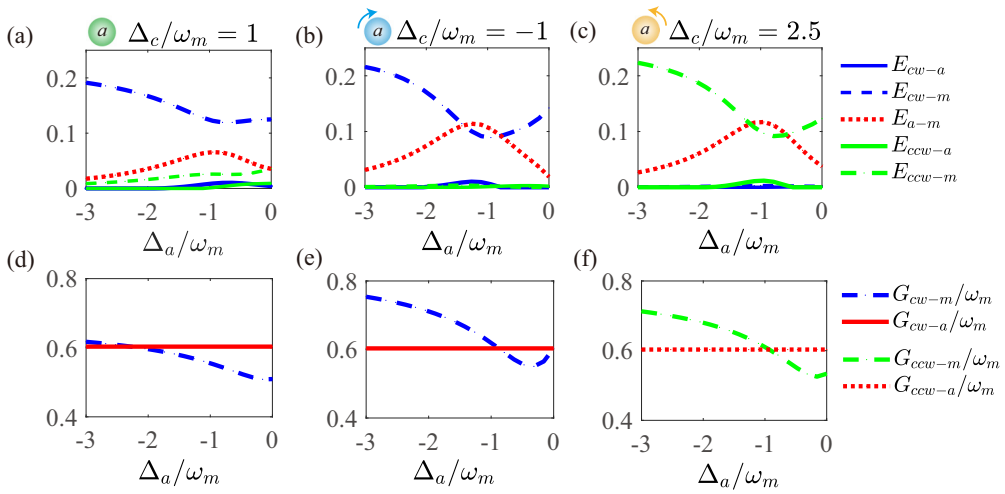

FIG. 2. Entanglement and coupling strengths of various two-mode subsystem vs atomic detuning in different driving situations and in which the optimal cavity detuning condition is satisfied. (a), (d) For the stationary resonator, $\Delta_c/\omega_m = 1$. (b), (e) For the rotation resonator under CW driving mode, $\Delta_c/\omega_m = -1$. (c), (f) For the rotation resonator under CCW driving mode, $\Delta_c/\omega_m = 2.5$.

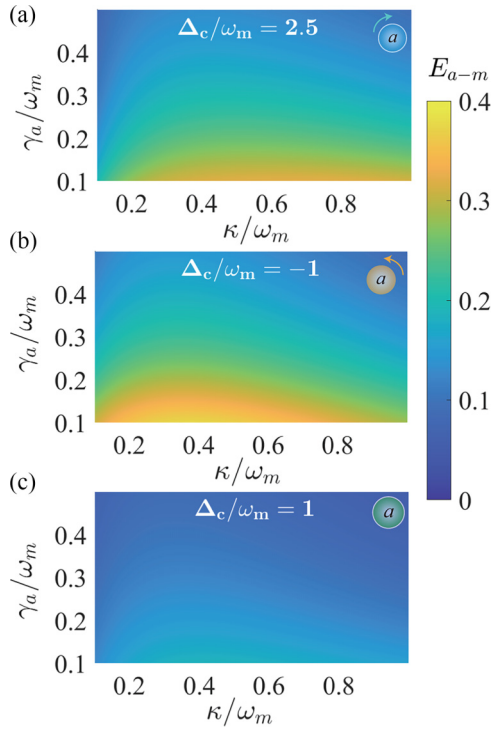

FIG. 3. Robustness of bipartite entanglement against noise in different driving situations. (a) For spinning resonator under CW driving mode, $\Delta_c/\omega_m = 2.5$ and $\Delta_a/\omega_m \simeq -1$. (b) For spinning resonator under CCW driving mode, $\Delta_c/\omega_m = -1$ and $\Delta_a/\omega_m \simeq -1$. (c) For stationary resonator, $\Delta_c/\omega_m = 1$ and $\Delta_a/\omega_m \simeq -1$.

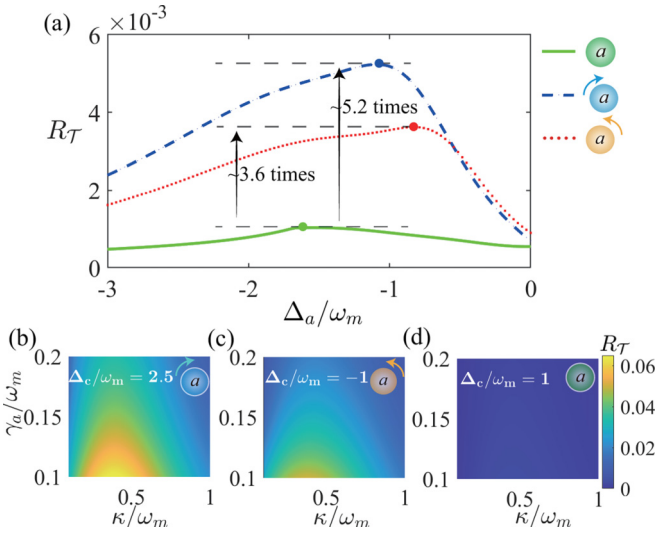

FIG. 4. (a) Nonreciprocal enhancement of tripartite entanglement for atomic ensemble, optical cavity, and mechanical oscillator. The parameters are chosen as $\Omega = 30$ kHz, $P = 40$ mW, $\Delta_c/\omega_m = -2.5$ for the spinning resonator under CW driving mode, $\Delta_c/\omega_m = -1$ for the spinning resonator under CCW driving mode, and $\Delta_c/\omega_m = 1$ for the stationary resonator. (b)–(d) The robustness of tripartite entanglement against noise in different driving situations. The optimal cavity detuning conditions and atomic detuning conditions for different driving situations are satisfied, respectively.

entanglement [Figs. 3(a) and 3(b)] is larger than in the stationary resonator [Fig. 3(c)] with the same cavity decay and the atom spontaneous radiation. These results suggest that the nonreciprocal effect significantly enhances the robustness of bipartite entanglement against noise.

B. Tripartite entanglement

After discussing the nonreciprocal enhancement effect on bipartite entanglement, we now investigate the impact of the nonreciprocal effect on the tripartite entanglement. In Fig. 3(a), we, respectively, plot the minimal residual contangle $R_{\mathcal{T}}^{i|jk}$ versus the atom detuning Δ_a for the stationary resonator and the spinning resonator driven from the opposite directions. At $\Delta_a/\omega_m \simeq -1$, the tripartite entanglement among the driven cavity mode, atomic mode, and mechanical mode reaches the maximal value. This is because the redistribution of entanglement leads to those bipartite entanglements reaching a relatively balanced value, which results in the tripartite entanglement maximal.

Compared with the stationary system, the nonreciprocal effect in the spinning system also enlarges the tripartite entanglement due to the enhanced bipartite entanglement transfer process. As shown in Fig. 4(a), the maximized value of tripartite entanglement for the spinning resonator driven by the CW mode ($\Delta_c/\omega_m = -1$) is about 5.2 times the maximized value for the stationary resonator. The maximized value for the spinning resonator driven from the opposite direction ($\Delta_c/\omega_m = 2.5$) is about 3.6 times. In addition to the enhancement effect of entanglement, the obtained nonreciprocal entanglement is also more robust against the environmental noise of the system. In Figs. 4(b) and 4(c), we, respectively, plot $R_{\mathcal{T}}^{i|jk}$ of the spinning resonator versus the decay of cavity κ and atom γ_a in different driving situations, where both the optimal cavity and atomic detuning conditions have been satisfied. However, the value of tripartite entanglement is very low for the stationary resonator, i.e., always less than 0.01 in Fig. 4(d). This indicates that the nonreciprocal effect can significantly enhance the robustness against noise. The maximal value of whole tripartite entanglement can reach more than 0.06 at an appropriate damping rate for the CW driving and 0.05 for the CCW driving, as shown in Figs. 4(b) and 4(c). That means that we can generate the maximized nonreciprocal tripartite entanglement by optimizing the system parameters in the spinning system.

As we all know, the macroscopic entanglement is particularly sensitive to temperature. Therefore, we go on to discuss the robustness of nonreciprocal macroscopic entanglement to the environment temperature. For the bipartite entanglement in our system, we choose the entanglement between the atomic ensemble and mechanical oscillator E_{a-m} as an example. In Fig. 5(a), we, respectively, plot the bipartite entanglement E_{a-m} versus temperature for the stationary and spinning resonator to investigate the temperature robustness of the atom-mechanical entanglement E_{a-m}.

We find that although the nonreciprocal atom-mechanical entanglement is stronger than the stationary system, it is also fragile to temperature. As shown in Fig. 5(a), the entanglement in the stationary system vanishes near 3 K, while in the spinning system, the entanglement vanishes near 1.5 K for the

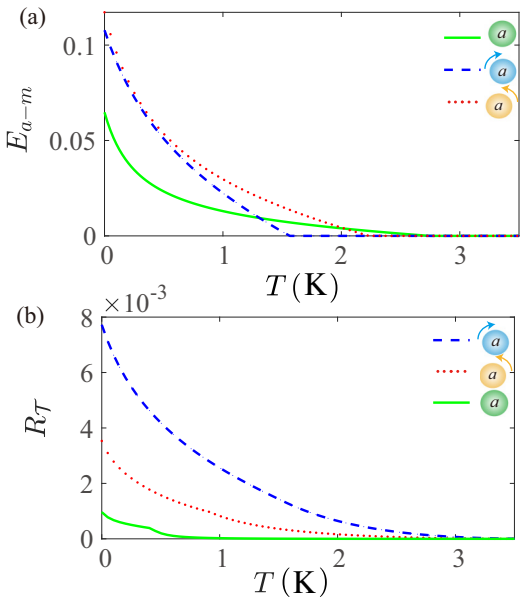

FIG. 5. (a) Temperature robustness of atom-mechanical entanglement in different driving situations. (b) Temperature robustness of tripartite entanglement in different driving situations.

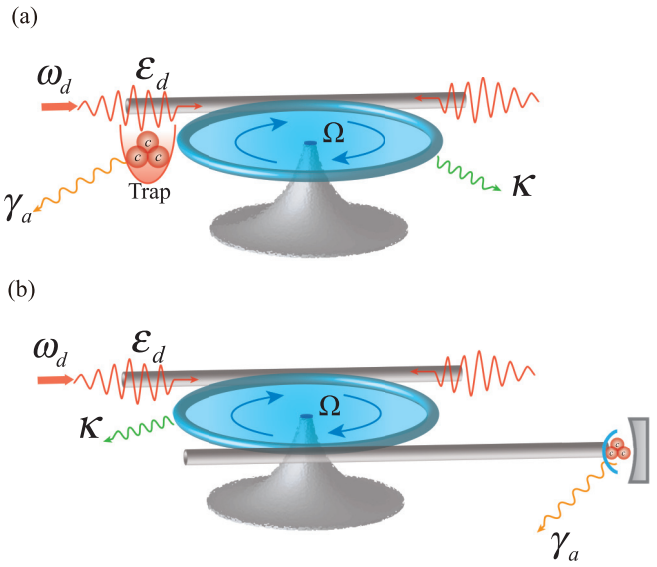

FIG. 6. Two experimentally feasible setup diagrams. (a) Direct coupling between resonator and atomic ensemble. The atomic ensemble is loaded in a magnetic trap or optical trap. (b) Indirect coupling between resonator and atomic ensemble. The atomic ensemble is trapped in a fiber-based Fabry-Perot cavity and this fiber simultaneously couples with the resonator.

CW driving and 2.2 K for the CCW driving. Namely, the temperature robustness of atom-mechanical entanglement in the nonreciprocal effect is weaker. This is because of the increase in effective optomechanical coupling for the spinning resonator, which is evident in Figs. 2(d)–2(f). The larger effective optomechanical coupling means that the thermal environment has a greater influence on the system. This is because the low-frequency mechanical oscillator is the primary source of thermal environmental noise. However, the results are quite different when studying the robustness of the tripartite entanglement. In Fig. 5(b), the tripartite entanglement versus temperature is shown. We can see that the nonreciprocal effect not only enhances the tripartite entanglement at low temperatures, but also makes it more robust against temperature. The tripartite entanglement vanishes near 0.7 K for the stationary resonator, but the nonreciprocal tripartite entanglement is still entangled above 2 K, whatever the driving situation is. This suggests that the generated nonreciprocal tripartite entanglement is more noise tolerant.

IV. EXPERIMENTAL FEASIBILITY

In this section, we discuss the experimental feasibility of our theoretical model. Experimentally, the resonator spins fast enough to split its countercirculating optical mode, achieving the nonreciprocal propagation of light in a spinning whispering-gallery-mode resonator evanescently coupled with a tapered fiber [68]. Before long, the nonreciprocal entanglement between the mechanical oscillator and optical cavity was investigated in a similar system [59]. Based on that experimental and theoretical research, we selected the experimentally feasible parameters for the WGM resonator. The radius and angular velocity of a microdisk are $R = 1.1$ mm and $\Omega = 30$ kHz, respectively. The quality factor of the optical cavity mode is $Q = 3.2 \times 10^7$ and, correspondingly, the decay rate is $\kappa = 38$ MHz. The frequency and decay rate of the mechanical mode are $\omega_m = 63$ MHz and $\gamma_m = 5.2$ kHz, respectively. In our theoretical mode, the coupling between the atomic ensemble and microdisk resonator may be a challenging problem. Here, we discuss two possible schemes to achieve our proposal as follows.

First, we give a direct coupling scheme. As shown in Fig. 6(a), the atomic ensemble can be loaded into a magnetic trap or optical trap to couple it to the WGM resonator by the optical evanescent field. In this scheme, the atomic ensemble is a cloud of dilute atomic gas, which is optically precooled and loaded into a magnetic trap or optical dipole trap in a vacuum. After evaporative cooling, the atomic ensemble can form a condensate consisting of approximately 10^6 atoms through the Bose-Einstein condensate (BEC) phase transition [81–83]. The coupling between the WGM cavity and atom by the optical evanescent field has been reported experimentally [84–86]. As already confirmed in experiments [86], by employing a deep standing-wave optical dipole trap, the coupling between atom and resonator is achieved, where the atomic dipole decay rate is $\gamma_a = 2\pi \times 3$ MHz and the coupling strength is $g \approx 2\pi \times 10$ MHz.

On the other hand, the atomic ensemble can also be coupled to the WGM resonator via indirect interaction. As shown in Fig. 6(b), the atomic ensemble is trapped in a fiber-based Fabry-Perot cavity and simultaneously couples the fiber with the WGM resonator, resulting in the indirect coupling between the atomic ensemble and resonator. The scheme of trapping the atomic ensemble inside a fiber-based Fabry-Perot cavity has already been realized in experiment [87]. In this experiment, the atomic ensemble forms a BEC in a magnetic trap by evaporative cooling, and the BEC is positioned in the

fiber-based Fabry-Perot mode. Each of the atoms is identically and strongly coupled to the cavity mode, where the single-atom coupling strength is $g = 2\pi \times 215$ MHz and the atomic decay rate is $\gamma_a = 2\pi \times 3$ MHz. In addition, the coupling between the fiber and the WGM resonator has already been demonstrated [88,89]. In our scheme, the selected atomic collective coupling strength is $G_a = 38$ MHz and, correspondingly, the single-atom coupling strength is $g \approx 10^4$ Hz ($G_a = g\sqrt{N_a}$) for the atomic ensemble formed by hundreds of thousands of atoms. Meanwhile, the atomic decay rate is set as $\gamma_a = G_a$. Compared to the previous theoretical and experimental works, those chosen parameters are experimental feasibility in our proposal.

V. CONCLUSION

In conclusion, we have achieved nonreciprocal bipartite and tripartite macroscopic entanglement, explored the enhancement effects of entanglement, and assessed the robustness of entanglement against various types of noise. The origins of nonreciprocal and enhanced entanglement are elucidated: the nonreciprocity of macroscopic entanglement stems from breaking time-reversal symmetry via the Sagnac effect. Concurrently, the enhancement of nonreciprocal macroscopic entanglement results from competitive coupling dynamics within the system. Achieving competitive equilibrium facilitates significant entanglement redistribution from cavity-mechanical to atom-mechanical subsystems, thereby enhancing tripartite entanglement in our proposal. Moreover, we investigated the noise tolerance of both bipartite and tripartite entanglement and found them to exhibit robustness against environmental noise. Regarding temperature robustness, we observed that bipartite entanglement is enhanced at low temperatures, but becomes fragile at higher temperatures. Conversely, tripartite entanglement demonstrates reversed temperature robustness, being more resilient to environmental noise even at higher temperatures. Furthermore, we discussed the experimental feasibility of our proposal, which combines optical nonreciprocal effects with a compound COM system. The outcomes of our study are instrumental in advancing the understanding of quantum characteristics in macroscopic compound systems. Importantly, our proposed scheme offers significant potential for engineering various quantum effects and establishing practical quantum networks.

ACKNOWLEDGMENTS

This work was supported by the National Natural Science Foundation of China (Grants No. 12204424, No. 12147149, No. 12147156, No. 12274376, No. 12074346, No. U21A20434, No. 11935006, No. 11774086), the China Postdoctoral Science Foundation (Grant No. 2022M722889), the Natural Science Foundation of Henan Province (Grant No. 212300410085), the Hunan Provincial Major Sci-Tech Program (Grant No. 2023ZJ1010), and the Science and Technology Innovation Program of Hunan Province (Grant No. 2020RC4047).

APPENDIX: DERIVATION OF THE LINEARIZED DYNAMICS

When the CCW mode is driven, the effective Hamiltonian of the system is given by

$$\begin{aligned} H = &\sum_{j=cw,ccw} \hbar\Delta_j a_j^\dagger a_j + \hbar\Delta_a S_+ S_- + \frac{\hbar\omega_m}{2}(p^2+q^2) \\ &- \hbar G_0(a_{cw}^\dagger a_{cw} + a_{ccw}^\dagger a_{ccw})q + (\hbar g a_{cw} S_+ + \hbar g a_{ccw} S_+ \\ &+ i\hbar\epsilon a_{ccw}^\dagger + \text{H.c.}). \end{aligned} \tag{A1}$$

By considering damping and noise terms from the external environment, a set of nonlinear Langevin equations can be derived as

$$\begin{aligned} \dot{q} &= \frac{1}{i\hbar}[q, H] = \omega_m p, \\ \dot{p} &= \frac{1}{i\hbar}[p, H] - \gamma_m p + \xi \\ &= -\omega_m q + G_0(a_{cw}^\dagger a_{cw} + a_{ccw}^\dagger a_{ccw}) - \gamma_m p + \xi, \\ \dot{a}_{cw} &= \frac{1}{i\hbar}[a_{cw}, H] - \kappa a_{cw} + \sqrt{2\kappa}a_{cw}^{in} \\ &= -(i\Delta_{cw} + \kappa)a_{cw} + iG_0 q a_{cw} - iG_a c + \sqrt{2\kappa}a_{cw}^{in}, \\ \dot{a}_{ccw} &= \frac{1}{i\hbar}[a_{ccw}, H] - \kappa a_{ccw} + \sqrt{2\kappa}a_{ccw}^{in} \\ &= -(i\Delta_{ccw} + \kappa)a_{ccw} + iG_0 q a_{ccw} - iG_a c + \sqrt{2\kappa}a_{ccw}^{in} \\ &\quad + \epsilon, \\ \dot{c} &= \frac{1}{i\hbar}[c, H] - \gamma_a c + \sqrt{2\gamma_a}F_c \\ &= -(i\Delta_a + \gamma_a)c - iG_a(a_{cw} + a_{ccw}) + \sqrt{2\gamma_a}F_c. \end{aligned} \tag{A2}$$

Each system operator can be rewritten as a steady-state value plus a fluctuation operator with zero-mean value with a strength driven laser. i.e., $q = q_s + \delta q$, $p = p_s + \delta p$, $a_j = \alpha_j + \delta a_j$, $c = c_s + \delta c$. By inserting these expressions into the nonlinear Langevin Eq. (A2) and decoupling these equations, a set of equations of steady-state value and a set of equations for the fluctuation operators can be derived as

$$\begin{aligned} p_s &= 0, \\ q_s &= \frac{G_0(|\alpha_{cw}|^2 + |\alpha_{ccw}|^2)}{\omega_m}, \\ \alpha_{cw} &= \frac{-iG_a c_s}{i\tilde{\Delta}_{cw} + \kappa}, \\ \alpha_{ccw} &= \frac{-iG_a c_s + \epsilon}{i\tilde{\Delta}_{ccw} + \kappa}, \\ c_s &= \frac{-iG_a(\alpha_{ccw} + \alpha_{cw})}{i\Delta_a + \gamma_a}, \end{aligned} \tag{A3}$$

and

$$\begin{aligned} \delta\dot{q} &= \omega_m \delta p, \\ \delta\dot{p} &= -\omega_m \delta q + G_0(\alpha_{cw}^\dagger \delta a_{cw} + \alpha_{cw}\delta a_{cw}^\dagger + \alpha_{ccw}^\dagger \delta a_{ccw} \\ &\quad + \alpha_{ccw}\delta a_{ccw}^\dagger) - \gamma_m \delta p + \xi, \end{aligned}$$

$$
\begin{aligned}
\delta\dot{a}_{cw} &= -(i\Delta_{cw}+\kappa)\delta a_{cw} + iG_0(q_s\delta a_{cw}+\alpha_{cw}\delta q) - iG_a\delta c \\
&\quad + \sqrt{2\kappa}a^{in}_{cw}, \\
\delta\dot{a}_{ccw} &= (i\Delta_{ccw}+\kappa)\delta a_{ccw} + iG_0(q_s\delta a_{ccw}+\alpha_{ccw}\delta q) - iG_a\delta c \\
&\quad + \sqrt{2\kappa}a^{in}_{ccw}, \\
\delta\dot{c} &= -(\gamma_a+i\Delta_a)\delta c - iG_a(\delta a_{cw}+\delta a_{ccw}) + \sqrt{2\gamma_a}F_c,
\end{aligned} \tag{A4}
$$

where $\tilde{\Delta}_j = \Delta_j - G_0 q_s$. The quadratures of fluctuation and noise operators are defined by

$$
\begin{aligned}
\delta X_j &= \frac{1}{\sqrt{2}}(\delta a_j^\dagger + \delta a_j), \quad \delta Y_j = \frac{i}{\sqrt{2}}(\delta a_j^\dagger - \delta a_j), \\
\delta x &= \frac{1}{\sqrt{2}}(\delta c^\dagger + \delta c), \quad \delta y = \frac{i}{\sqrt{2}}(\delta c^\dagger - \delta c), \\
X_j^{in} &= \frac{1}{\sqrt{2}}\left(a_j^{in,\dagger} + a_j^{in}\right), \quad Y_j^{in} = \frac{i}{\sqrt{2}}\left(a_j^{in,\dagger} - a_j^{in}\right), \\
x_{in} &= \frac{1}{\sqrt{2}}\left(F_c^{in,\dagger} + F_c^{in}\right), \quad y_{in} = \frac{i}{\sqrt{2}}\left(F_c^{in,\dagger} - F_c^{in}\right).
\end{aligned} \tag{A5}
$$

By combining Eqs. (A3) and (A4), we can obtain the dynamical equation of the quadratures of fluctuation operators,

$$
\begin{aligned}
\delta\dot{q} &= \omega_m\delta p, \\
\delta\dot{p} &= -\omega_m\delta q + G^x_{cw}\delta X_{cw} + G^y_{cw}\delta Y_{cw} + G^x_{ccw}\delta X_{ccw} \\
&\quad + G^y_{ccw}\delta Y_{ccw} - \gamma_m\delta p + \xi, \\
\delta\dot{X}_{cw} &= -\kappa\delta X_{cw} + \tilde{\Delta}_{cw}\delta Y_{cw} + G_a\delta y - G^y_{cw}\delta q + \sqrt{2\kappa}X^{in}_{cw}, \\
\delta\dot{Y}_{cw} &= -\tilde{\Delta}_{cw}\delta X_{cw} - \kappa\delta Y_{cw} + G_{cw}\delta q - G_a\delta x + G^x_{cw}\delta q \\
&\quad + \sqrt{2\kappa}Y^{in}_{cw}, \\
\delta\dot{X}_{ccw} &= -\kappa\delta X_{ccw} + \tilde{\Delta}_{ccw}\delta Y_{ccw} + G_a\delta y - G^y_{ccw}\delta q \\
&\quad + \sqrt{2\kappa}X^{in}_{ccw}, \\
\delta\dot{Y}_{ccw} &= -\tilde{\Delta}\delta X_{ccw} - \kappa\delta Y_{ccw} + G_{ccw}\delta q - G_a\delta x + G^x_{ccw} \\
&\quad + \sqrt{2\kappa}Y^{in}_{ccw}, \\
\delta\dot{x} &= G_a(\delta Y_{ccw} + \delta Y_{cw}) - \gamma_a\delta x + \Delta_a\delta y + \sqrt{2\gamma_a}X_{in}, \\
\delta\dot{y} &= -G_a(\delta X_{ccw} + \delta X_{cw}) - \Delta_a\delta x - \gamma_a\delta y + \sqrt{2\gamma_a}y_{in}.
\end{aligned} \tag{A6}
$$

Here, G^x_j and G^y_j are the real and imaginary parts of the linearized optomechanical coupling strength, i.e., $G_{j-m} = G^x_j + iG^y_j = \sqrt{2}G_0\alpha_j$. G_{cw-m} and G_{ccw-m} are the linearized optomechanical coupling strength for the CW optical mode and CCW optical mode, respectively. We define the vectors of the quadratures of fluctuation operators and input noise operators, $u^T(t) = (\delta X_{ccw}, \delta Y_{ccw}, \delta X_{cw}, \delta Y_{cw}, \delta x, \delta y, \delta q, \delta p)$ and $v^T(t) = (\sqrt{2\kappa}X^{in}_{ccw}, \sqrt{2\kappa}Y^{in}_{ccw}, \sqrt{2\kappa}X^{in}_{cw}, \sqrt{2\kappa}Y^{in}_{cw}, \sqrt{2\gamma_a}x_{in}, \sqrt{2\gamma_a}y_{in}, 0, \xi)$. Equation (A6) can be written in compact form as $\dot{u}(t) = Au(t) + v(t)$, where

$$
A = \begin{pmatrix}
-\kappa & \tilde{\Delta}_{ccw} & 0 & 0 & 0 & G_a & -G^y_{ccw} & 0 \\
-\tilde{\Delta}_{ccw} & -\kappa & 0 & 0 & -G_a & 0 & G^x_{ccw} & 0 \\
0 & 0 & -\kappa & \tilde{\Delta}_{cw} & 0 & G_a & -G^y_{cw} & 0 \\
0 & 0 & -\tilde{\Delta}_{cw} & -\kappa & -G_a & 0 & G^x_{cw} & 0 \\
0 & G_a & 0 & G_a & -\gamma_a & \Delta_a & 0 & 0 \\
-G_a & 0 & -G_a & 0 & -\Delta_a & -\gamma_a & 0 & 0 \\
0 & 0 & 0 & 0 & 0 & 0 & 0 & \omega_m \\
G^x_{ccw} & G^y_{ccw} & G^x_{cw} & G^y_{cw} & 0 & 0 & -\omega_m & -\gamma_m
\end{pmatrix}. \tag{A7}
$$

This is the same as Eq. (8) in the main text.

[1] R. Horodecki, P. Horodecki, M. Horodecki, and K. Horodecki, Rev. Mod. Phys. **81**, 865 (2009).

[2] A. G. J. MacFarlane, J. P. Dowling, and G. J. Milburn, Phil. Trans. R. Soc. London A **361**, 1655 (2003).

[3] D. Vitali, S. Gigan, A. Ferreira, H. R. Böhm, P. Tombesi, A. Guerreiro, V. Vedral, A. Zeilinger, and M. Aspelmeyer, Phys. Rev. Lett. **98**, 030405 (2007).

[4] X. Zhang, H.-O. Li, G. Cao, M. Xiao, G.-C. Guo, and G.-P. Guo, Natl. Sci. Rev. **6**, 32 (2019).

[5] U. Andersen, G. Leuchs, and C. Silberhorn, Laser. Photon. Rev. **4**, 337 (2010).

[6] M. A. Nielsen and I. L. Chuang, *Quantum Computation and Quantum Information: 10th Anniversary Edition* (Cambridge University Press, Cambridge, 2010).

[7] F. Flamini, N. Spagnolo, and F. Sciarrino, Rep. Prog. Phys. **82**, 016001 (2019).

[8] C. L. Degen, F. Reinhard, and P. Cappellaro, Rev. Mod. Phys. **89**, 035002 (2017).

[9] D. Bouwmeester, A. Ekert, and A. Zeilinger, *The Physics of Quantum Information* (Springer, Berlin, 2000).

[10] J. M. Raimond, M. Brune, and S. Haroche, Rev. Mod. Phys. **73**, 565 (2001).

[11] J.-W. Pan, Z.-B. Chen, C.-Y. Lu, H. Weinfurter, A. Zeilinger, and M. Żukowski, Rev. Mod. Phys. **84**, 777 (2012).

[12] N. Friis, G. Vitagliano, M. Malik, and M. Huber, Nat. Rev. Phys. **1**, 72 (2019).

[13] L. Hackermüller, K. Hornberger, B. Brezger, A. Zeilinger, and M. Arndt, Nature (London) **427**, 711 (2004).

[14] B. Julsgaard, A. Kozhekin, and E. S. Polzik, Nature (London) **413**, 400 (2001).

[15] S. Kotler, G. A. Peterson, E. Shojaee, F. Lecocq, K. Cicak, A. Kwiatkowski, S. Geller, S. Glancy, E. Knill, R. W. Simmonds, J. Aumentado, and J. D. Teufel, Science **372**, 622 (2021).

[16] L. M. de Lépinay, C. F. Ockeloen-Korppi, M. J. Woolley, and M. A. Sillanp, Science **372**, 625 (2021).

[17] M. Aspelmeyer, T. J. Kippenberg, and F. Marquardt, Rev. Mod. Phys. **86**, 1391 (2014).

[18] H. Xiong, L.-G. Si, X. Lv, X. Yang, and Y. Wu, Sci. China Phys. Mech. Astron. **58**, 1 (2015).

[19] S. Barzanjeh, A. Xuereb, S. Gröblacher, M. Paternostro, C. Regal, and E. Weig, Nat. Phys. **18**, 15 (2022).

[20] J. Zhang, K. Peng, and S. L. Braunstein, Phys. Rev. A **68**, 013808 (2003).

[21] S. Huang and G. S. Agarwal, New J. Phys. **11**, 103044 (2009).

[22] D.-Y. Wang, C.-H. Bai, Y. Xing, S. Liu, S. Zhang, and H.-F. Wang, Phys. Rev. A **102**, 043705 (2020).

[23] H. Yu, L. McCuller, M. Tse, N. Kijbunchoo, L. Barsotti, N. Mavalvala, and members of the LIGO Scientific Collaboration, Nature (London) **583**, 43 (2020).

[24] J.-Q. Liao and L. Tian, Phys. Rev. Lett. **116**, 163602 (2016).

[25] Y. Wang, H.-L. Zhang, J.-L. Wu, J. Song, K. Yang, W. Qin, H. Jing, and L.-M. Kuang, Sci. China Phys. Mech. Astron. **66**, 110311 (2023).

[26] S.-B. Tang, H. Qin, B.-B. Liu, D.-Y. Wang, K. Cui, S.-L. Su, L.-L. Yan, and G. Chen, Phys. Rev. A **108**, 053514 (2023).

[27] Q. Zheng, J. Xu, Y. Yao, and Y. Li, Phys. Rev. A **94**, 052314 (2016).

[28] B.-B. Li, L. Ou, Y. Lei, and Y.-C. Liu, Nanophoton. **10**, 2799 (2021).

[29] A.-N. Xu and Y.-C. Liu, Phys. Rev. A **106**, 013506 (2022).

[30] M. A. Page, M. Goryachev, H. Miao, Y. Chen, Y. Ma, D. Mason, M. Rossi, C. D. Blair, L. Ju, D. G. Blair, A. Schliesser, M. E. Tobar, and C. Zhao, Commun. Phys. **4**, 27 (2021).

[31] D.-G. Lai, F. Zou, B.-P. Hou, Y.-F. Xiao, and J.-Q. Liao, Phys. Rev. A **98**, 023860 (2018).

[32] D.-G. Lai, J.-F. Huang, X.-L. Yin, B.-P. Hou, W. Li, D. Vitali, F. Nori, and J.-Q. Liao, Phys. Rev. A **102**, 011502(R) (2020).

[33] K. Jähne, C. Genes, K. Hammerer, M. Wallquist, E. S. Polzik, and P. Zoller, Phys. Rev. A **79**, 063819 (2009).

[34] E. E. Wollman, C. U. Lei, A. J. Weinstein, J. Suh, A. Kronwald, F. Marquardt, A. A. Clerk, and K. C. Schwab, Science **349**, 952 (2015).

[35] H. Xie, C.-G. Liao, X. Shang, M.-Y. Ye, and X.-M. Lin, Phys. Rev. A **96**, 013861 (2017).

[36] J. Li, S.-Y. Zhu, and G. S. Agarwal, Phys. Rev. Lett. **121**, 203601 (2018).

[37] M. Pinard, A. Dantan, D. Vitali, O. Arcizet, T. Briant, and A. Heidmann, Europhys. Lett. **72**, 747 (2005).

[38] D. Vitali, S. Mancini, and P. Tombesi, J. Phys. A: Math. Theor. **40**, 8055 (2007).

[39] C. Genes, D. Vitali, and P. Tombesi, Phys. Rev. A **77**, 050307(R) (2008).

[40] Y. Wu, J.-H. Liu, Y.-F. Yu, Z.-M. Zhang, and J.-D. Wang, Phys. Rev. Appl. **20**, 034043 (2023).

[41] C.-H. Dong, Z. Shen, C.-L. Zou, Y.-L. Zhang, W. Fu, and G.-C. Guo, Nat. Commun. **6**, 6193 (2015).

[42] J. Kim, M. C. Kuzyk, K. Han, H. Wang, and G. Bahl, Nat. Phys. **11**, 275 (2015).

[43] K. Xia, F. Nori, and M. Xiao, Phys. Rev. Lett. **121**, 203602 (2018).

[44] L. Tang, J. Tang, M. Chen, F. Nori, M. Xiao, and K. Xia, Phys. Rev. Lett. **128**, 083604 (2022).

[45] S. Manipatruni, J. T. Robinson, and M. Lipson, Phys. Rev. Lett. **102**, 213903 (2009).

[46] Z. Shen, Y.-L. Zhang, Y. Chen, C.-L. Zou, Y.-F. Xiao, X.-B. Zou, F.-W. Sun, G.-C. Guo, and C.-H. Dong, Nat. Photon. **10**, 657 (2016).

[47] N. R. Bernier, L. D. Tóth, A. Koottandavida, M. A. Ioannou, D. Malz, A. Nunnenkamp, A. K. Feofanov, and T. J. Kippenberg, Nat. Commun. **8**, 604 (2017).

[48] L. Mercier de Lépinay, E. Damskägg, C. F. Ockeloen-Korppi, and M. A. Sillanpää, Phys. Rev. Appl. **11**, 034027 (2019).

[49] X.-W. Xu, J.-Q. Liao, H. Jing, and L.-M. Kuang, Sci. China Phys. Mech. Astron. **66**, 100312 (2023).

[50] B. Bahari, A. Ndao, F. Vallini, A. E. Amili, Y. Fainman, and B. Kanté, Science **358**, 636 (2017).

[51] Y. Jiang, S. Maayani, T. Carmon, F. Nori, and H. Jing, Phys. Rev. Appl. **10**, 064037 (2018).

[52] R. Huang, A. Miranowicz, J.-Q. Liao, F. Nori, and H. Jing, Phys. Rev. Lett. **121**, 153601 (2018).

[53] D.-Y. Wang, L.-L. Yan, S.-L. Su, C.-H. Bai, H.-F. Wang, and E. Liang, Opt. Express **31**, 22343 (2023).

[54] Y.-H. Zhou, X.-Y. Zhang, T. Liu, Q.-C. Wu, Z.-C. Shi, H.-Z. Shen, and C.-P. Yang, Phys. Rev. Appl. **18**, 064009 (2022).

[55] Y. Shen, M. Bradford, and J.-T. Shen, Phys. Rev. Lett. **107**, 173902 (2011).

[56] M.-X. Dong, K.-Y. Xia, W.-H. Zhang, Y.-C. Yu, Y.-H. Ye, E.-Z. Li, L. Zeng, D.-S. Ding, B.-S. Shi, G.-C. Guo, and F. Nori, Sci. Adv. **7**, eabe8924 (2021).

[57] S.-Y. Ren, W. Yan, L.-T. Feng, Y. Chen, Y.-K. Wu, X.-Z. Qi, X.-J. Liu, Y.-J. Cheng, B.-Y. Xu, L.-J. Deng, G.-C. Guo, L. Bi, and X.-F. Ren, Laser Photon. Rev. **16**, 2100595 (2022).

[58] Y.-F. Jiao, J.-X. Liu, Y. Li, R. Yang, L.-M. Kuang, and H. Jing, Phys. Rev. Appl. **18**, 064008 (2022).

[59] Y.-F. Jiao, S.-D. Zhang, Y.-L. Zhang, A. Miranowicz, L.-M. Kuang, and H. Jing, Phys. Rev. Lett. **125**, 143605 (2020).

[60] J. Chen, X.-G. Fan, W. Xiong, D. Wang, and L. Ye, Phys. Rev. B **108**, 024105 (2023).

[61] J.-X. Liu, Y.-F. Jiao, Y. Li, X.-W. Xu, Q.-Y. He, and H. Jing, Sci. China Phys. Mech. Astron. **66**, 230312 (2023).

[62] Q. Zheng, W. Zhong, G. Cheng, and A. Chen, Opt. Commun. **546**, 129796 (2023).

[63] S.-B. Lee, J. Yang, S. Moon, S.-Y. Lee, J.-B. Shim, S. W. Kim, J.-H. Lee, and K. An, Phys. Rev. Lett. **103**, 134101 (2009).

[64] E. Verhagen and A. Alù, Nat. Phys. **13**, 922 (2017).

[65] W. Chen, Y. Lu, S. Zhang, K. Zhang, G. Huang, M. Qiao, X. Su, J. Zhang, J.-N. Zhang, L. Banchi, M. S. Kim, and K. Kim, Nat. Phys. **19**, 877 (2023).

[66] J. Sheng, X. Wei, C. Yang, and H. Wu, Phys. Rev. Lett. **124**, 053604 (2020).

[67] X. Ren, J. Pan, M. Yan, J. Sheng, C. Yang, Q. Zhang, H. Ma, Z. Wen, K. Huang, H. Wu, and H. Zeng, Nat. Commun. **14**, 5037 (2023).

[68] S. Maayani, R. Dahan, Y. Kligerman, E. Moses, A. U. Hassan, H. Jing, F. Nori, D. N. Christodoulides, and T. Carmon, Nature (London) **558**, 569 (2018).

[69] G. B. Malykin, Phys.-Usp. **43**, 1229 (2000).
[70] X. Chen, Y.-C. Liu, P. Peng, Y. Zhi, and Y.-F. Xiao, Phys. Rev. A **92**, 033841 (2015).
[71] S.-l. Ma, P.-b. Li, A.-p. Fang, S.-y. Gao, and F.-l. Li, Phys. Rev. A **88**, 013837 (2013).
[72] P. Z. Crispin Gardiner, *Quantum Noise* (Springer, Berlin, 2000).
[73] E. X. DeJesus and C. Kaufman, Phys. Rev. A **35**, 5288 (1987).
[74] Y.-H. Ma and L. Zhou, J. Appl. Phys. **111**, 103109 (2012).
[75] G. Adesso, A. Serafini, and F. Illuminati, Phys. Rev. A **70**, 022318 (2004).
[76] R. Simon, Phys. Rev. Lett. **84**, 2726 (2000).
[77] D.-G. Lai, J.-Q. Liao, A. Miranowicz, and F. Nori, Phys. Rev. Lett. **129**, 063602 (2022).
[78] G. Adesso and F. Illuminati, J. Phys. A: Math. Theor. **40**, 7821 (2007).
[79] G. Adesso and F. Illuminati, New J. Phys. **8**, 15 (2006).
[80] V. Coffman, J. Kundu, and W. K. Wootters, Phys. Rev. A **61**, 052306 (2000).
[81] D. S. Jin, J. R. Ensher, M. R. Matthews, C. E. Wieman, and E. A. Cornell, Phys. Rev. Lett. **77**, 420 (1996).
[82] E. A. Cornell, C. Monroe, and C. E. Wieman, Phys. Rev. Lett. **67**, 2439 (1991).
[83] A. H. Abbas, X. Meng, R. S. Patil, J. A. Ross, A. G. Truscott, and S. S. Hodgman, Phys. Rev. A **103**, 053317 (2021).
[84] T. Aoki, B. Dayan, E. Wilcut, W. P. Bowen, A. S. Parkins, T. J. Kippenberg, K. J. Vahala, and H. J. Kimble, Nature (London) **443**, 671 (2006).
[85] B. Dayan, A. S. Parkins, T. Aoki, E. P. Ostby, K. J. Vahala, and H. J. Kimble, Science **319**, 1062 (2008).
[86] E. Will, L. Masters, A. Rauschenbeutel, M. Scheucher, and J. Volz, Phys. Rev. Lett. **126**, 233602 (2021).
[87] Y. Colombe, T. Steinmetz, G. Dubois, F. Linke, D. Hunger, and J. Reichel, Nature (London) **450**, 272 (2007).
[88] M. Cai, O. Painter, and K. J. Vahala, Phys. Rev. Lett. **85**, 74 (2000).
[89] S. M. Spillane, T. J. Kippenberg, O. J. Painter, and K. J. Vahala, Phys. Rev. Lett. **91**, 043902 (2003).